MNRAS **000**, 1–7 (2019) Preprint 26 February 2019 Compiled using MNRAS LaTeX style file v3.0

Bow shocks, bow waves, and dust waves. I. Strong coupling limit

William J. Henney & S. Jane Arthur
Instituto de Radioastronomía y Astrofísica, Universidad Nacional Autónoma de México, Apartado Postal 3-72, 58090 Morelia, Michoacán, México

Accepted XXX. Received YYY; in original form ZZZ

ABSTRACT
Dust waves and bow waves result from the action of a star's radiation pressure on a stream of dusty plasma that flows past it. They are an alternative mechanism to hydrodynamic bow shocks for explaining the curved arcs of infrared emission seen around some stars. When gas and grains are perfectly coupled, for a broad class of stellar parameters, wind-supported bow shocks predominate when the ambient density is below $100\,\mathrm{cm}^{-3}$ to $1000\,\mathrm{cm}^{-3}$. At higher densities radiation-supported bows can form, tending to be optically thin bow waves around B stars, or optically thick bow shocks around early O stars.

Key words: circumstellar matter – radiation: dynamics – stars: winds, outflows

1 INTRODUCTION

Curved emission arcs around stars (e.g., Gull & Sofia 1979) are often interpreted as *bow shocks*, due to a supersonic hydrodynamic interaction between the star's wind and an external stream. This stream may be due to the star's own motion or to an independent flow, such as an H II region in the champagne phase (Tenorio-Tagle 1979), or another star's wind (Canto et al. 1996). However, an alternative interpretation in some cases may be a radiation-pressure driven bow wave, as first proposed by van Buren & McCray (1988, §VI). In this scenario (see Fig. 1), photons emitted by the star are absorbed by dust grains in the incoming stream, with the resultant momentum transfer being sufficient to decelerate and deflect the grains within a certain distance from the star, forming a dust-free, bow-shaped cavity with an enhanced dust density at its edge.

Two regimes are possible, depending on the strength of coupling between the gas (or plasma) and the dust. In the strong-coupling regime, gas–grain drag decelerates the gas along with the dust. If the stream is optically thin to the star's ultraviolet radiation, then the deceleration occurs gradually over a range of radii, forming a relatively thick shell. On the other hand, if the stream is optically thick, then a shocked gas shell forms in a similar fashion to the wind-driven bow shock case, except internally supported by trapped radiation instead of shocked stellar wind. In the weak-coupling regime, the gas stream is relatively unaffected and the dust temporarily decouples to form a dust-only shell. This second case has recently been studied in detail in the context of the interaction of late O-type stars (some of which have very weak stellar winds) with dusty photoevaporation flows inside H II regions (Ochsendorf et al. 2014b,a; Ochsendorf & Tielens 2015). We follow the nomenclature proposed by Ochsendorf et al. (2014a), in which *dust wave* refers to the weak coupling case and *bow wave* to the strong coupling case. More complex, hybrid scenarios are also possible, such as that studied by van Marle et al. (2011), where a hydrodynamic bow shock forms, but the larger dust grains that accompany the stellar wind pass right through the shocked gas shell, and form their own dust wave at a larger radius.

This is the first in a series of papers where we develop simple physical models to show in detail when and how these different interaction regimes apply when varying the parameters of the star, the dust grains, and the ambient stream. We concentrate primarily on the case of luminous early type stars, where dust is present only in the ambient stream, and not in the stellar wind. In this first paper, we consider the case where the grains are perfectly coupled to the gas via collisions. The following two papers consider the decoupling of grains and gas in a sufficiently strong radiation field (Henney & Arthur 2019a, Paper II), and how observations can distinguish between different classes of bow (Henney & Arthur 2019b, Paper III). The paper is organized as follows. In § 2 we propose a simple model for stellar bows and investigate the relative importance of wind and radiation in providing internal support for the bow shell as a function of the density and velocity of the ambient stream, and for different types of star. In § 3 we calculate the physical state of the bow shell, considering under what circumstances it can trap within itself the star's ionization front and how efficient radiative cooling will be. In § **??** we briefly discuss the application of our models to observed bows. In § **??** we summarise the conclusions of our study.

2 A SIMPLE MODEL FOR STELLAR BOWS

We consider the canonical case of a bow around a star of bolometric luminosity, L, with a radiatively driven wind, which is immersed in an external stream of gas and dust with density, ρ, and velocity, v. The size and shape of the bow is determined by a generalized balance of pressure (or, equivalently, momentum) between internal and external sources. We assume that the stream is supersonic and super-alfvenic, so that the external pressure is dominated by the ram pressure, ρv^2, and that dust grains and gas are perfectly coupled by collisions (the breakdown of this assumption is the topic of Paper II).

Although dust grains typically constitute only a small fraction $Z_{\mathrm{d}} \sim 0.01$ of the mass of the external stream, they nevertheless dominate the broad-band opacity at FUV, optical and IR wavelengths

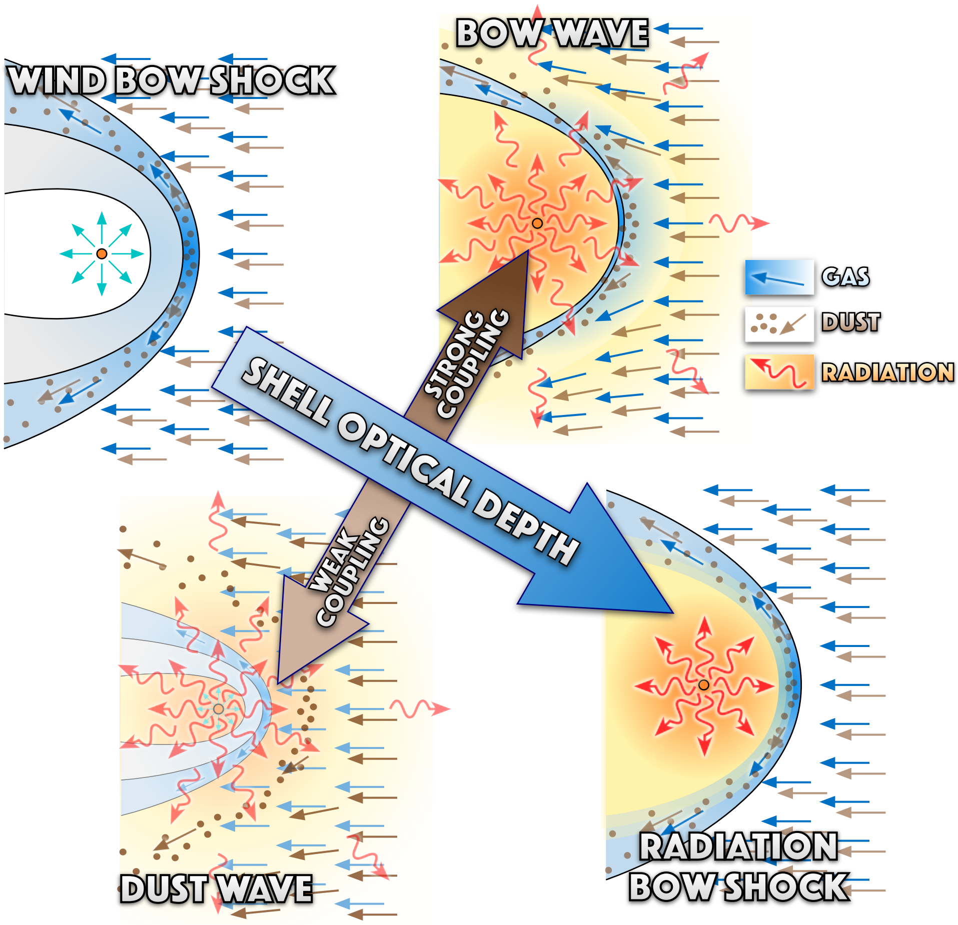

Figure 1. Regimes in the supersonic interaction of a luminous star with its environment. When radiation effects are unimportant, we have the standard (magneto-)hydrodynamical wind-supported bow shock (upper left), where the ram pressure of the stellar wind balances the ram pressure of the oncoming stream. As the optical depth of the shocked shell increases, the stellar radiation momentum adds to the wind ram pressure to help support the bow. If the shell is completely opaque to stellar radiation, we have a radiation-supported bow shock (lower right), where it is the stellar radiation pressure that balances the ram pressure of the external stream. For intermediate optical depths, we have two cases depending on the strength of coupling between grains and gas. If the coupling is strong, then we have a radiation-supported bow wave (upper right), where the plasma stream as a whole is gradually radiatively decelerated as it approaches the star. If the coupling is weak, then the radiation momentum is felt only by the dust, which decouples from the gas to form a dust wave, with the gas stream continuing inward to form a wind-supported bow shock closer to the star. Note that the gas–grain coupling is both direct (via collisions) and indirect (via the magnetic field) (see Paper II).

if they are present.[1] The strong coupling assumption means that all the radiative forces applied to the dust grains are directly felt by the gas also.

2.1 Bows supported by radiation and wind

The internal pressure is the sum of wind ram pressure and the effective radiation pressure that acts on the bow shell. The radiative momentum loss rate of the star is L/c and the wind momentum loss rate can be expressed as

$$\dot{M}V = \eta_{\mathrm{w}} L/c\,, \tag{1}$$

where η_{w} is the momentum efficiency of the wind, which is typically < 1 (Lamers & Cassinelli 1999). If the optical depth is very large, then all of the stellar radiative momentum, emitted with rate L/c, is trapped by the bow shell. In the single scattering limit,[2] and temporarily neglecting the wind for clarity of exposition, then

[1] At EUV wavelengths ($\lambda < 912$ Å), gas opacity dominates if the hydrogen neutral fraction is larger than ≈ 0.001, see discussion of ionization front trapping below.

[2] Although it may seem inconsistent to assume single scattering in the case of high optical depths, this is defensible for the following reasons. (1) The grain albedo is not that high (typically ~ 0.5 at ultraviolet through optical wavelengths). (2) The scattered radiation field is more isotropic than the stellar field, leading to cancellation in the radiative flux. (3) Absorbed

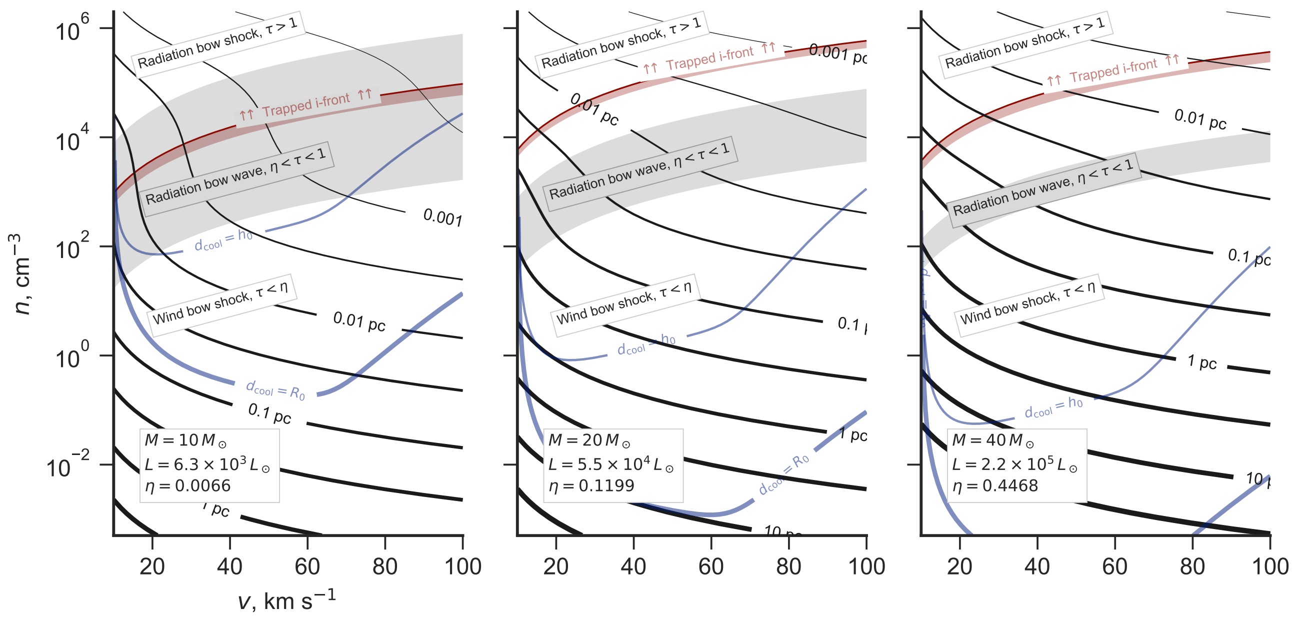

Figure 2. Bow regimes in parameter space (v, n) of the external stream for main-sequence OB stars of different masses: (a) 10 M$_\odot$, (b) 20 M$_\odot$, (c) 40 M$_\odot$. In all cases, $\kappa = 600\,\mathrm{cm^2\,g^{-1}}$ and efficient gas-grain coupling is assumed. Solid black lines of varying width show the bow size (star-apex separation, R_0), while gray shading shows the radiation bow wave regime, with lower border $\tau = \eta_\mathrm{w}$ and upper border $\tau = 1$, where $\tau = 2\kappa\rho R_0$ is the optical depth through the bow. For bows above the red solid line, the ionization front is trapped inside the bow. Blue lines delineate different cooling regimes. Above the thin blue line ($d_\mathrm{cool} = h_0$), the bow shock radiates efficiently, forming a thin shocked shell. Below the thick blue line ($d_\mathrm{cool} = R_0$), the bow shock is essentially non-radiative.

pressure balance at the bow apex, a distance R_0 along the symmetry axis from the star is given by

$$\frac{L}{4\pi c R_0^2} = \rho v^2\,, \tag{2}$$

which yields a fiducial bow shock radius in this optically thick, radiation-only limit as

$$R_* = \left(\frac{L}{4\pi c \rho v^2}\right)^{1/2}\,. \tag{3}$$

We now consider the opposite, optically thin limit. If the total opacity (gas plus dust) per total mass (gas plus dust) is κ (with units of cm^2 g^{-1}), then the radiative acceleration is

$$a_\mathrm{rad} = \frac{\kappa L}{4\pi c R^2}\,. \tag{4}$$

Therefore, an incoming stream with initial velocity, v_∞, can be brought to rest by radiation alone at a distance R_{**} where

$$\int_{R_{**}}^{\infty} a_\mathrm{rad}\, dr = \tfrac{1}{2} v_\infty^2\,, \tag{5}$$

yielding

$$R_{**} = \frac{\kappa L}{2\pi c v_\infty^2}\,. \tag{6}$$

On the other hand, we can also argue as in the optically thick case above by approximating the bow shell as a surface, and balancing stellar radiation pressure against the ram pressure of the incoming stream. The important difference when the shell is not optically thick is that only a fraction $1 - e^{-\tau}$ of the radiative momentum is absorbed by the bow, so that equation (2) is replaced with

$$\frac{L(1 - e^{-\tau})}{4\pi c R_0^2} = \rho v^2\,. \tag{7}$$

In the optically thin limit, $1 - e^{-\tau} \approx \tau$, so these two descriptions can be seen to agree ($R_0 \to R_{**}$) so long as

$$\tau = 2\kappa\rho R_0\,, \tag{8}$$

which we will assume to hold generally.

Then, defining a fiducial optical depth,

$$\tau_* = \rho\kappa R_*\,, \tag{9}$$

and now reinstating the stellar wind ram pressure term from equation (1), we find that the general bow radius can be written in terms of the fiducial radius as

$$R_0 = x R_*\,, \tag{10}$$

where x is the solution of

$$x^2 - \left(1 - e^{-2\tau_* x}\right) - \eta_\mathrm{w} = 0\,. \tag{11}$$

Since this is a transcendental equation, x must be found numerically, but we can write explicit expressions for three limiting cases:

$$x \approx \begin{cases} \text{if } \tau_* \gg 1: & (1 + \eta_\mathrm{w})^{1/2} \\ \text{if } \tau_*^2 \ll 1: & \tau_* + \left(\tau_*^2 + \eta_\mathrm{w}\right)^{1/2} \approx \begin{cases} \text{if } \tau_*^2 \gg \eta_\mathrm{w}: & 2\tau_* \\ \text{if } \tau_*^2 \ll \eta_\mathrm{w}: & \eta_\mathrm{w}^{1/2} \end{cases} \end{cases} \tag{12}$$

The first case, $x \approx (1 + \eta_\mathrm{w})^{1/2}$, corresponds to a *radiation bow shock* (RBS); the second case, $x \approx 2\tau_*$, corresponds to a *radiation*

radiation is re-emitted at infrared wavelengths, where the dust opacity is very much lower.

bow wave (RBW); and the third case, $x \approx \eta_w^{1/2}$, corresponds to a *wind bow shock* (WBS). The two bow shock cases are similar in that the external stream is oblivious to the presence of the star until it suddenly hits the bow shock shell, differing only in whether it is radiation or wind that is providing the internal pressure. In the intermediate bow wave case, on the other hand, the external stream is gradually decelerated by absorption of photons as it approaches the bow.[3]

2.2 Dependence on stellar type

We now consider the application to bow shocks around main sequence OB stars, as well as cool and hot supergiants, expressing stellar and ambient parameters in terms of typical values as follows:

$$\begin{aligned}
\dot{M}_{-7} &= \dot{M} / \left(10^{-7}\,\mathrm{M_\odot\,yr^{-1}}\right) \\
V_3 &= V / \left(1000\,\mathrm{km\,s^{-1}}\right) \\
L_4 &= L / \left(10^4\,\mathrm{L_\odot}\right) \\
v_{10} &= v_\infty / \left(10\,\mathrm{km\,s^{-1}}\right) \\
n &= (\rho / \bar{m}) / \left(1\,\mathrm{cm^{-3}}\right) \\
\kappa_{600} &= \kappa / \left(600\,\mathrm{cm^2\,g^{-1}}\right),
\end{aligned}$$

where $\bar{m}$ is the mean mass per hydrogen nucleon ($\bar{m} \approx 1.3 m_\mathrm{p} \approx 2.17 \times 10^{-24}$ g for solar abundances). Note that $\kappa = 600\,\mathrm{cm^2\,g^{-1}}$ corresponds to a cross section of $\approx 10^{-21}\,\mathrm{cm^2}$ per hydrogen nucleon, which is typical for interstellar medium dust (Bertoldi & Draine 1996) at far ultraviolet wavelengths, where OB stars emit most of their radiation. In terms of these parameters, we can express the stellar wind momentum efficiency as

$$\eta_\mathrm{w} = 0.495\, \dot{M}_{-7}\, V_3\, L_4^{-1} \tag{13}$$

and the fiducial radius and optical depth as

$$R_* / \mathrm{pc} = 2.21\, (L_4 / n)^{1/2}\, v_{10}^{-1} \tag{14}$$

$$\tau_* = 0.0089\, \kappa_{600}\, (L_4\, n)^{1/2}\, v_{10}^{-1}\,. \tag{15}$$

In Figure 2, we show results for the bow size (apex distance, R_0) as a function of the density, n, and relative velocity, v_∞, of the external stream, with each panel corresponding to a particular star, with parameters as shown in Table 1. To facilitate comparison with previous work, we choose stellar parameters similar to those used in the hydrodynamical simulations of Meyer et al. (2014, 2016, 2017), based on stellar evolution tracks for stars of $10\,\mathrm{M_\odot}$, $20\,\mathrm{M_\odot}$ and $40\,\mathrm{M_\odot}$ (Brott et al. 2011) and theoretical wind prescriptions (de Jager et al. 1988; Vink et al. 2000). Although the stellar parameters do evolve with time, they change relatively little during the main-sequence lifetime of several million years.[4] The three examples are an early B star ($10\,\mathrm{M_\odot}$), a late O star ($20\,\mathrm{M_\odot}$), and an early O star ($40\,\mathrm{M_\odot}$), which cover the range of luminosities and wind strengths expected from bow-producing hot main sequence stars. The luminosity is a steep function of stellar mass ($L \sim M^{2.5}$) and the wind mass-loss rate is a steep function of luminosity ($\dot{M} \sim L^{2.2}$), which means that the wind momentum efficiency is also a steep function of mass ($\eta_\mathrm{w} \sim M^3$), approaching unity for early O stars, but falling to less than 1% for B stars.

It can be seen from Figure 2 that the onset of the radiation bow wave regime is very similar for the three main-sequence stars, occurring at $n > 20$ to $40\, v_{10}^2$. An important difference, however, is that for the $40\,\mathrm{M_\odot}$ star, which has a powerful wind, the radiation bow wave regime only occurs for a very narrow range of densities, whereas for the $10\,\mathrm{M_\odot}$ star, with a much weaker wind, the regime is much broader, extending to $n < 10^4\, v_{10}^2$. Another difference is the size scale of the bows in this regime, which is $R_0 = 0.001$ pc to 0.003 pc for the $10\,\mathrm{M_\odot}$ star if $v_\infty = 40\,\mathrm{km\,s^{-1}}$, but $R_0 \approx 0.1$ pc for the $40\,\mathrm{M_\odot}$ star, assuming the same inflow velocity.

Figure 3 shows results for a cool M-type super-giant star with stellar parameters inspired by Betelgeuse (α Orionis), as listed in Table 1. Unlike the UV-dominated spectrum of the hot stars, this star emits predominantly in the near-infrared, where the dust extinction efficiency is lower, so we adopt a lower opacity of $60\,\mathrm{cm^2\,g^{-1}}$. This

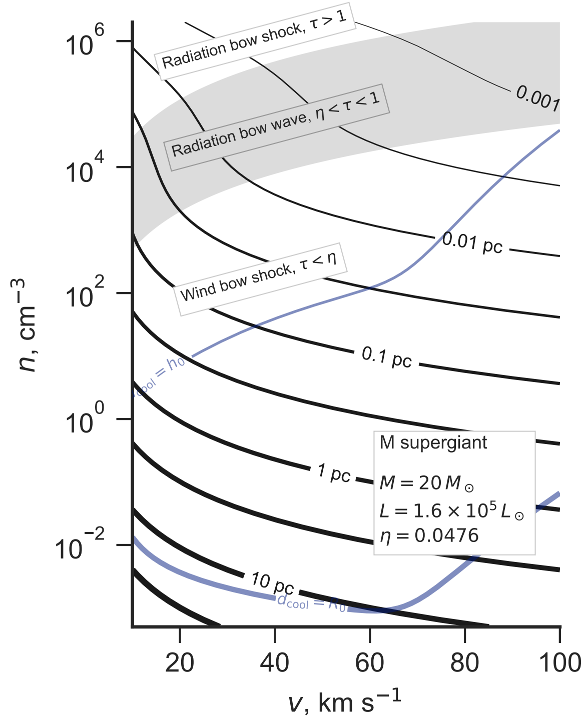

Figure 3. As Fig. 2, but for a cool M-type supergiant instead of hot main sequence stars. A smaller dust opacity is used, $\kappa = 60\,\mathrm{cm^2\,g^{-1}}$, because of the reduced extinction efficiency at the optical/infrared wavelengths emitted by this star.

[3] A shock can still form in this case, but shocked material constitutes only a small fraction of the total column density of the shell.

[4] Note that we have recalculated the stellar wind terminal velocities, since the values given in the Meyer et al. papers are troublingly low. We have used the prescription $V = 2.6 V_\mathrm{esc}$, where $V_\mathrm{esc} = (2GM(1 - \Gamma_e)/R)^{1/2}$ is the photospheric escape velocity, which is appropriate for strong line-driven winds with $T_\mathrm{eff} > 21\,000$ K (Lamers et al. 1995). We find velocities of $2500\,\mathrm{km\,s^{-1}}$ to $3300\,\mathrm{km\,s^{-1}}$, which are consistent with observations and theory (Vink et al. 1999) for O stars, but at least two times higher than those cited by Meyer et al. (2014). For main-sequence B stars, wind column densities are too low to reliably measure the terminal velocity from near ultraviolet P Cygni profiles (Prinja 1989), and so the values are theory-dependent (Krtička 2014) and hence more uncertain. A further complication is the existence of a subset of OB stars with anomalously weak winds (Puls et al. 2008), which in some cases is related to the presence of strong (∼ 1 kG) magnetic fields (Oskinova et al. 2011).

Table 1. Stellar parameters for example stars

	$M/\mathrm{M}_\odot$	L_4	$\dot{M}_{-7}$	V_3	η_w	Sp. Type	T_eff/kK	λ_eff / μm	S_{49}	Figures
	10	0.63	0.0034	2.47	0.0066	B1.5 V	25.2	0.115	0.000 13	2a, ??a, ??– ??
Main-sequence OB stars	20	5.45	0.492	2.66	0.1199	O9 V	33.9	0.086	0.16	2b, ??b
	40	22.2	5.1	3.31	0.4468	O5 V	42.5	0.068	1.41	2c, ??c
Blue supergiant star	33	30.2	20.2	0.93	0.3079	B0.7 Ia	23.5	0.123	0.016	4
Red supergiant star	20	15.6	100	0.015	0.0476	M1 Ia	3.6	0.805	0	3

has the effect of shifting the radiation bow wave regime to higher densities: $n = 1000$ to $30\,000\,v_{10}^2$ in this case.

2.3 Effects of stellar gravity

In principle, gravitational attraction from the star, of mass M, will partially counteract the radiative acceleration. This can be accounted for by replacing L with an effective luminosity

$$L_\mathrm{eff} = L\left(1 - \Gamma_\mathrm{E}^{-1}\right) , \tag{16}$$

in which Γ_E is the Eddington factor:

$$\Gamma_\mathrm{E} = \frac{\kappa L}{4\pi c G M} = 458.5\,\frac{\kappa_{600} L_4}{M} , \tag{17}$$

where, in the last expression, M is measured in solar masses. For the stars in Table 1, we find $\Gamma_\mathrm{E} \approx 30$ to 400, so gravity can be safely ignored. The only exception is when the optical depth of the bow is very large: $\tau > \ln \Gamma_\mathrm{E} \sim 5$, in which case gravity may be important in the outer parts of the shell (see Rodríguez-Ramírez & Raga 2016).

3 PHYSICAL STATE OF THE BOW SHELL

3.1 Ionization state

In this section we calculate whether the star is capable of photoionizing the entire bow shock shell, or whether the ionization front will be trapped within it. The number of hydrogen recombinations[5] per unit time per unit area in a fully ionized shell is

$$\mathcal{R} = \alpha_\mathrm{B} n_\mathrm{sh}^2 h_\mathrm{sh} , \tag{18}$$

while the advective flux of hydrogen nuclei through the shock is

$$\mathcal{A} = n v , \tag{19}$$

and the flux of hydrogen-ionizing photons ($h\nu > 13.6\,\mathrm{eV}$) incident on the inner edge of the shell is

$$\mathcal{F} = \frac{S}{4\pi R_0^2} , \tag{20}$$

where S is the ionizing photon luminosity of the star. Any shell with $\mathcal{R} + \mathcal{A} > \mathcal{F}$ cannot be entirely photoionized by the star, and so must have trapped the ionization front.

The ratio of advective particle flux to ionizing flux is, from equations (3), (19), (20),

$$\frac{\mathcal{A}}{\mathcal{F}} = 5.86 \times 10^{-5}\,\frac{x^2 L_4}{v_{10} S_{49}} , \tag{21}$$

[5] The diffuse field is treated in the on-the-spot approximation, assuming all emitted Lyman continuum photons are immediately re-absorbed locally, so the case B recombination co-efficient, $\alpha_\mathrm{B} = 2.6 \times 10^{-13}\,T_4^{-0.7}\,\mathrm{cm^3\,s^{-1}}$, is used, where $T_4 = T/10^4$ K.

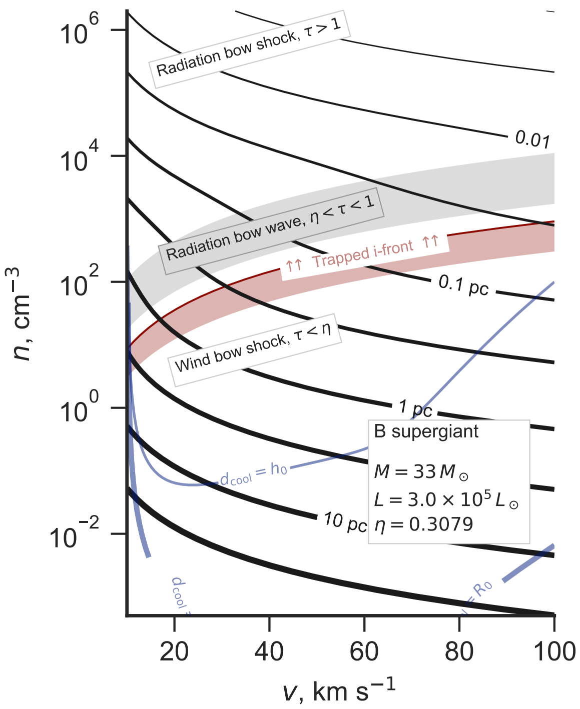

Figure 4. As Fig. 2, but for an evolved B-type supergiant instead of main sequence stars. This is similar to the early O MS star of Fig. 2c in many respects, except for the trapping of the ionization front, which occurs for much lower outer stream densities.

where

$$S_{49} = S/\left(10^{49}\,\mathrm{s^{-1}}\right) .$$

Numerical values of S_{49} for our three example stars are given in Table 1, taken from Figure 4 of Sternberg et al. (2003). Since $\mathcal{A} \ll \mathcal{F}$ in nearly all cases, for clarity of exposition we ignore $\mathcal{A}$ in the following discussion, although it is included in quantitative calculations. The column density of the shocked shell can be found, for example, from equations (10) and (12) of Wilkin (1996) in the limit $v_\infty/V \to 0$ (Wilkin's parameter α) and $\theta \to 0$. This yields

$$n_\mathrm{sh} h_\mathrm{sh} = \tfrac{3}{4} n R_0 . \tag{22}$$

Assuming strong cooling behind the shock,[6] the shell density is

$$n_\mathrm{sh} = \mathcal{M}_0^2 n \tag{23}$$

where $\mathcal{M}_0 = v_\infty / c_\mathrm{s}$ is the isothermal Mach number of the external

[6] This is shown to be justified in § 3.2.

stream.[7] Putting these together with equations (3) and (9), one finds that $\mathcal{R} > \mathcal{F}$ implies

$$x^3 \tau_* > \frac{4 S c c_s \bar{m}^2 \kappa}{3 \alpha L} \, . \tag{24}$$

From equation (11), it can be seen that x depends on the external stream parameters, n, v_∞ only via τ_*, and so equation (24) is a condition for τ_*, which, by using equation (15), becomes a condition on n/v_{10}^2. In the radiation bow shock case, $x = (1 + \eta_{\rm w})^{1/2}$, and the condition can be written:

$$\text{RBS:} \quad \frac{n}{v_{10}^2} > 2.65 \times 10^8 \, \frac{S_{49}^2 T_4^{3.4}}{L_4^3 (1 + \eta_{\rm w})^3} \, . \tag{25}$$

In the radiation bow wave case, $x = 2\tau_*$, and the condition can be written:

$$\text{RBW:} \quad \frac{n}{v_{10}^2} > 5.36 \times 10^4 \, \frac{S_{49}^{1/2} T_4^{0.85}}{\kappa_{600}^{3/2} L_4^{3/2}} \, . \tag{26}$$

In the wind bow shock case, the result is the same as equation (25), but changing the factor $(1 + \eta_{\rm w})^3$ to $\eta_{\rm w}^3$. For the example hot stars in Table 1, and assuming $\kappa_{600} = 1$, $T_4 = 0.8$, the resulting density threshold is $n > (1000 \text{ to } 5000)\, v_{10}^2$, depending only weakly on the stellar parameters, which is shown by the red lines in Figure 2. For the $10\,\mathrm{M}_\odot$ star, this is in the radiation bow wave regime, whereas for the higher mass stars it is in the radiation bow shock regime. When the external stream is denser than this, then the outer parts of the shocked shell may be neutral instead of ionized, giving rise to a cometary compact H II region (Mac Low et al. 1991; Arthur & Hoare 2006). This is only necessarily true, however, when the star is isolated. If the star is in a cluster environment, then the contribution of other nearby massive stars to the ionizing radiation field must be considered.

Quite different results are obtained for a B-type supergiant star (see Tab. 1 and Fig. 4), which has a similar bolometric luminosity and wind strength to the $40\,\mathrm{M}_\odot$ main-sequence star, but a hundred times lower ionizing luminosity. This results in a far lower threshold for trapping the ionization front of $n > 40 v_{10}^2$. The advective flux, $\mathcal{A}$, is relatively stronger for this star than for the main-sequence stars, but even for $v_{10} < 2$, where the effect is strongest, the change is only of order the width of the dark red line in Figure 4.

In principle, when the ionization front trapping occurs in the bow wave regime, then the curves for R_0 will be modified in the region above the red line because all of the ionizing radiation is trapped in the shell due to gas opacity, which is not included in equation (8). However, this only happens for our $10\,\mathrm{M}_\odot$ star, which has a relatively soft spectrum. Table 1 gives the peak wavelength of the stellar spectrum for this star as $\lambda_{\rm eff} = 0.115\,\mu\mathrm{m}$, which is significantly larger than the hydrogen ionization threshold at $0.0912\,\mu\mathrm{m}$, meaning that only a small fraction of the total stellar luminosity is in the EUV band and affected by the gas opacity. The effect on R_0 is therefore small. For the higher mass stars, $\lambda_{\rm eff} < 0.0912\,\mu\mathrm{m}$, so the majority of the luminosity is in the EUV band, but in these cases the ionization front trapping occurs well inside the radiation bow shock zone, where the dust optical depth is already sufficient to trap all of the radiative momentum.

[7] The sound speed depends on the temperature and hydrogen and helium ionization fractions, y and $y_{\rm He}$ as $c_s^2 = (1 + y + z_{\rm He} y_{\rm He})(kT/\bar{m})$, where $z_{\rm He}$ is the helium nucleon abundance by number relative to hydrogen and $k = 1.380\,650\,3 \times 10^{-16}\ \mathrm{erg\,K^{-1}}$ is Boltzmann's constant. We assume $y = 1$, $y_{\rm He} = 0.5$, $z_{\rm He} = 0.09$, so that $c_s = 11.4\, T_4^{1/2}\ \mathrm{km\,s^{-1}}$.

3.2 Efficiency of radiative cooling

In this section, we calculate whether the radiative cooling is sufficiently rapid behind the bow shock to allow the formation of a thin, dense shell. Since this is mainly a concern at low densities, where cooling is least efficient, we will assume that the wind bow shock regime applies unless otherwise specified. We label quantities just outside the shock by the subscript "0", quantities just inside the shock (after thermalization, but before any radiative cooling) by the subscript "1", and quantities after the gas has cooled back to the photoionization equilibrium temperature by the subscript "2". Assuming a ratio of specific heats, $\gamma = 5/3$, the relation between the pre-shock and immediate post-shock quantities is

$$\frac{n_1}{n_0} = \frac{4\mathcal{M}_0^2}{\mathcal{M}_0^2 + 3} \tag{27}$$

$$\frac{T_1}{T_0} = \tfrac{1}{16}\left(5\mathcal{M}_0^2 - 1\right)\left(1 + 3/\mathcal{M}_0^2\right) \tag{28}$$

$$\frac{v_1}{v_0} = \left(\frac{n_1}{n_0}\right)^{-1} , \tag{29}$$

where $\mathcal{M}_0 = v_0/c_s$. The cooling length of the post-shock gas can be written as

$$d_{\rm cool} = \frac{3 P_1 v_1}{2(\mathcal{L}_1 - \mathcal{G}_1)} , \tag{30}$$

where P_1 is the thermal pressure and $\mathcal{L}_1$, $\mathcal{G}_1$ are the volumetric radiative cooling and heating rates. For fully photoionized gas, we have $P_1 \approx 2 n_1 k T_1$, $\mathcal{L}_1 = n_1^2 \Lambda(T_1)$, and $\mathcal{G}_1 = n_1^2 \Gamma(T_1)$, where $\Lambda(T)$ is the cooling coefficient, which is dominated by metal emission lines that are excited by electron collisions, and $\Gamma(T)$ is the heating coefficient, which is dominated by hydrogen photo-electrons (Osterbrock & Ferland 2006). The cooling coefficient has a maximum around 10^5 K, and for typical ISM abundances can be approximated as follows:

$$\Lambda_{\rm warm} = 3.3 \times 10^{-24}\, T_4^{2.3}\ \mathrm{erg\,cm^3\,s^{-1}} \tag{31}$$

$$\Lambda_{\rm hot} = 10^{-20}\, T_4^{-1}\ \mathrm{erg\,cm^3\,s^{-1}} \tag{32}$$

$$\Lambda = \left(\Lambda_{\rm warm}^{-k} + \Lambda_{\rm hot}^{-k}\right)^{-1/k} \quad \text{with} \quad k = 3 , \tag{33}$$

which is valid in the range $0.7 < T_4 < 1000$. We approximate the heating coefficient as

$$\Gamma = 1.77 \times 10^{-24}\, T_4^{-1/2}\ \mathrm{erg\,cm^3\,s^{-1}} , \tag{34}$$

where the coefficient is chosen so as to give $\Gamma = \Lambda$ at an equilibrium temperature of $T_4 = 0.8$.

In Figure 2 we show curves calculated from equations (27) to (34), corresponding to $d_{\rm cool} = R_0$ (thick blue line) and $d_{\rm cool} = h_0$ (thin blue line), where h_0 is the shell thickness in the efficient cooling case. In this context, $n_0 = n$ and $n_2 = n_{\rm sh}$, so that h_0 follows from equations (22) and (23) as

$$h_0 = \tfrac{3}{4} \mathcal{M}_0^{-2} R_0 \, . \tag{35}$$

The bends in the curves at $v \approx 50\ \mathrm{km\,s^{-1}}$ are due to the maximum in the cooling coefficient $\Lambda(T)$ around 10^5 K. For bows with outer stream densities above the thin blue line, radiative cooling is so efficient that the bow shock can be considered isothermal, and so the shell is dense and thin (at least, in the apex region). It can be seen that the ionization front trapping always occurs at densities larger than this, which justifies the use of equation (23) in the previous section. For bows with outer stream densities below the thick blue line, cooling is unimportant and the bow shock can be considered non-radiative. In this case the shell is thicker than in the radiative case, $h_{\rm sh}/R_0 \approx 0.2$ to 0.3.[8] For bows with outer stream densities between the two blue lines, cooling does occur, albeit inefficiently, so that the shell thickness is set by $d_{\rm cool}$ rather than h_0.

REFERENCES

Arthur S. J., Hoare M. G., 2006, ApJS, 165, 283
Bertoldi F., Draine B. T., 1996, ApJ, 458, 222
Brott I., et al., 2011, A&A, 530, A115
Canto J., Raga A. C., Wilkin F. P., 1996, ApJ, 469, 729
Gull T. R., Sofia S., 1979, ApJ, 230, 782
Henney W. J., Arthur S. J., 2019a, MNRAS
Henney W. J., Arthur S. J., 2019b, MNRAS
Krtička J., 2014, A&A, 564, A70
Lamers H. J. G. L. M., Cassinelli J. P., 1999, Introduction to Stellar Winds. Cambridge, UK: Cambridge University Press
Lamers H. J. G. L. M., Snow T. P., Lindholm D. M., 1995, ApJ, 455, 269
Mac Low M.-M., van Buren D., Wood D. O. S., Churchwell E., 1991, ApJ, 369, 395
Meyer D. M.-A., Mackey J., Langer N., Gvaramadze V. V., Mignone A., Izzard R. G., Kaper L., 2014, MNRAS, 444, 2754
Meyer D. M.-A., van Marle A.-J., Kuiper R., Kley W., 2016, MNRAS, 459, 1146
Meyer D. M.-A., Mignone A., Kuiper R., Raga A. C., Kley W., 2017, MNRAS, 464, 3229
Ochsendorf B. B., Tielens A. G. G. M., 2015, A&A, 576, A2
Ochsendorf B. B., Cox N. L. J., Krijt S., Salgado F., Berné O., Bernard J. P., Kaper L., Tielens A. G. G. M., 2014a, A&A, 563, A65
Ochsendorf B. B., Verdolini S., Cox N. L. J., Berné O., Kaper L., Tielens A. G. G. M., 2014b, A&A, 566, A75
Oskinova L. M., Todt H., Ignace R., Brown J. C., Cassinelli J. P., Hamann W.-R., 2011, MNRAS, 416, 1456
Osterbrock D. E., Ferland G. J., 2006, Astrophysics of gaseous nebulae and active galactic nuclei, second edn. Sausalito, CA: University Science Books
Prinja R. K., 1989, MNRAS, 241, 721
Puls J., Vink J. S., Najarro F., 2008, A&ARv, 16, 209
Rodríguez-Ramírez J. C., Raga A. C., 2016, MNRAS, 460, 1876
Sternberg A., Hoffmann T. L., Pauldrach A. W. A., 2003, ApJ, 599, 1333
Tenorio-Tagle G., 1979, A&A, 71, 59
Vink J. S., de Koter A., Lamers H. J. G. L. M., 1999, A&A, 350, 181
Vink J. S., de Koter A., Lamers H. J. G. L. M., 2000, A&A, 362, 295
Wilkin F. P., 1996, ApJ, 459, L31
de Jager C., Nieuwenhuijzen H., van der Hucht K. A., 1988, A&AS, 72, 259
van Buren D., McCray R., 1988, ApJ, 329, L93
van Marle A. J., Meliani Z., Keppens R., Decin L., 2011, ApJ, 734, L26

This paper has been typeset from a TEX/LATEX file prepared by the author.

[8] An approximate value can be found from equation (22) by substituting $n = n_0$ and $n_{\rm sh} \approx n_1$, then using equation (27). Consideration of the slight increase in density between the shock and the contact/tangential discontinuity reduces this value by 5–10%.